ARTICLE

JAAS
www.rsc.org/jaas

Spectroscopic and electrical studies of a solution-cathode glow discharge

Michael R. Webb,[a] Francisco J. Andrade,[a] Gerardo Gamez,[a] Robert McCrindle[b] and Gary M. Hieftje*[a]

[a] *Department of Chemistry, Indiana University, Bloomington, IN 47405, USA. E-mail: hieftje@indiana.edu; Fax: 1-812-855-0958; Tel: 1-812-855-2189*

[b] *On leave from Tshwane University of Technology, Department of Chemistry and Physics, Private Bag X680, Pretoria, RSA 0001. E-mail: mccrindleri@tut.ac.za; Fax: +2712 318 6286; Tel: +2712 318 6290*

Received 18th March 2005, Accepted 26th July 2005
First published as an Advance Article on the web 1st September 2005

A glow discharge using a solution as the cathode was investigated to add to the understanding of the operating mechanism and characteristics of such systems. The intensities and vertical distributions of emission from several analytes and background species were observed and compared with the vertical distribution of Fe excitation and OH rotational temperatures, as well as to electrical characteristics. The effects of the discharge gap size, the pH and conductivity of the solution, the applied current and the solution flow rate on these distributions were also studied. Detection limits for this system were found to be comparable to those of similar systems and mostly in range of tens of parts per billion.

Introduction

Glow discharges have attracted increasing interest in recent years.[1] Both a cause and a result of this interest has been a broadening of samples that can be analyzed and an improvement in analytical performance. Gas-sampling discharges have permitted the analysis of flowing gases, and radiofrequency powering schemes have enabled the analysis of non-conductive solids and offered some advantages, such as more rapid stabilization in the analysis of conductive solids.[1,2] Pulsed discharges have enhanced ionization and emission, improved signal-to-background discrimination through gated detection, improved depth resolution, and allowed the molecular analysis of gases.[1,3,4]

Liquid samples present a greater challenge. Although cathodic sputtering introduces material from solid samples into the bulk of the discharge primarily as atoms, the relatively low gas temperatures are insufficient to desolvate liquid samples introduced into the bulk of the discharge. Additionally, water-related species lower the metastable population in the negative glow. For these reasons, most techniques have focused on drying a solution before introducing it into the glow discharge. Most commonly, this has been done by drying the sample onto a surface, which is then used as the glow discharge cathode. However, particle-beam devices and other nebulizers have also been used to desolvate flowing samples for analysis.[1,5,6] To preserve the glow discharge advantage of simplicity, a technique with comparable or superior performance but without the complexity of desolvation would be preferable.

The foundations for such a technique were laid down over a century ago, when Gubkin[7] introduced glow discharge electrolysis (GDE), a system in which a grounded electrolytic solution acts as the glow discharge cathode. In his studies and those which would follow over the next century, the focus was on the electrochemical reactions in the system, although Couch and Brenner[8] did observe emission from certain elements in the plasma. In recent years, GDE has also been used for surface modification.[9,10] The first use of GDE for analytical spectroscopy was in 1993 by Cserfalvi and co-workers,[11] who found that atomic emission was substantially enhanced at low pH. Their basic design consists of a glass capillary emerging upwards from a reservoir of electrolytic solution and a sample solution overflowing from the capillary into the reservoir. A glow discharge is sustained between the solution exiting the capillary and a metal anode a few millimetres above it. The pool of solution is grounded, and the electrical connection to the capillary exit is through the overflow, or a combination of the overflow and a salt bridge connecting the pool of solution to the solution within the capillary. In later papers, this design of GDE has been described as an electrolyte-cathode discharge (ELCAD).[12–26] Because of the necessity of the overflow connection in most designs, and because typical sample consumption is in the mL min^{-1} range, flow rates below 1.5 mL min^{-1} have not been reported and flow rates of about 8 mL min^{-1} are typical.

Variations on this idea have been introduced. A liquid-sampling atmospheric pressure glow discharge (LS-APGD) is designed similarly, but lacks the solution reservoir and instead uses a metal capillary in place of the glass one to electrically connect the solution.[27–29] It is not clear whether this difference fundamentally changes the discharge's mechanism. Moderate detection limits, all in the single parts per million range, have been reported for only a few elements so far, but LS-APGD solution flow rates can be significantly lower than ELCAD flow rates, and are typically less than 1 mL min^{-1}. A drop-spark discharge (DSD), which replaces the metal anode with a dripping electrolytic anode, is a pulsed source that operates similarly to the ELCAD.[26] Porous materials have also been used to create liquid-to-liquid discharges, but these discharges have not been used for analytical purposes and have exhibited quite different electrical characteristics.[30] Current fluctuations in a GDE system of a different design have also been used to detect both electrolytic and non-electrolytic compounds in a flowing sample.[31] A miniaturized ELCAD operating with sample flows below 5 μl min^{-1} has been described, but the source suffers from significant instabilities and the analytical performance has not yet been reported.[32]

DOI: 10.1039/b503961d

One attraction of a glow discharge source for solid sample analysis is its relatively low cost. ELCAD promises similar benefits. Notably, emission was enhanced in an air atmosphere compared with He or Ar atmospheres and detection limits were improved with an open system compared with a closed one.[18,20] Power requirements are low (typically under 75 W), a moderate resolution monochromator can be used due to a fairly uncomplicated spectrum, and the source itself is extremely inexpensive. Despite this low cost and the relative newness of ELCAD, reported detection limits mostly fall in the tens of parts per billion, with a few in the single parts per billion range.[23,24]

However, the characterization of the source is far from complete and there are limitations in its current form. The robustness of ELCAD is not yet known and there is disagreement about its operating mechanism.[9,13,25,28,29,33] Although the sample flow rate has been reduced since the technique's introduction, the 3–4 mL min^{-1} optimum found in a recent study is still several times higher than the eluent flow from a typical liquid chromatograph.[24] Further research characterizing the source in terms of its strengths, limitations, and mechanisms is clearly needed.

Experimental

A representation of the source cell is shown in Fig. 1. This cell is simpler than the design of most other ELCAD cells. The solution enters the cell through a 1-mL serological pipette which has been bent so the tip points upwards. Above this tip is a 1.6-mm diameter Ti anode to which a positive potential is applied through a 400-Ω ballast resistor. The solution overflows from the tip into an approximately 35 mL reservoir containing a grounded graphite electrode. This overflow creates an electrical connection between the solution at the pipette's tip and the graphite electrode. The position of the Ti anode is reproducibly controlled by means of a micrometer stage. To initiate the discharge, the anode is brought near (approximately 1 mm) to the solution while a high potential (1–2 kV) is applied to it; however, a Tesla-coil spark can also be used. A rectangular black polyethylene divider supported by the pipette serves multiple purposes. It reduces the amount of hydrogen (produced at the graphite cathode) that reaches the discharge by impeding its path through the air, it blocks some background light from sources external to the discharge, and it wicks moisture over the sides of the reservoir so a constant solution level is maintained within the reservoir. The hydrogen is blocked intentionally because its presence has been known to lower emission in other glow discharges; the light is blocked to reduce background noise, and the reservoir level is held constant to prevent fluctuations in the voltage between the pipette tip and the graphite cathode.

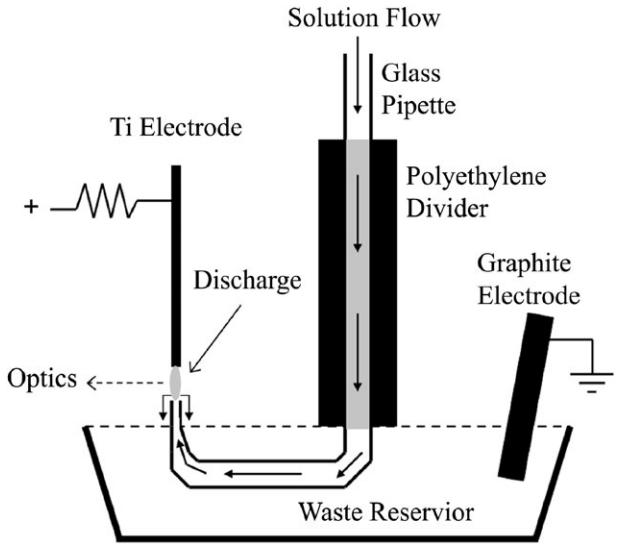

Fig. 1 Diagrammatic representation of solution-cathode glow discharge.

The sample solution is supplied by a syringe pump (Harvard Apparatus PHD 2000 (Holliston, MA)) at a typical flow of 3.5 mL min^{-1}. The discharge is powered by a Kepco (Flushing, NY) BHK 2000-0.1MG high-voltage power supply operated in constant-current mode, typically at 80 mA. For a similarly designed cell, the effects of geometry and flow on the resistive drop between the pipette tip and the location of the graphite electrode were studied without a discharge present. A Cole-Palmer (Chicago, IL) digital conductivity meter Model 1481-60 with custom platinum electrodes was used for these measurements. The resistance of a material is directly proportional to its length and inversely proportional to its cross-sectional area. The resistance of the cell was found to be directly proportional to the height of the pipette tip above the solution in the reservoir (*i.e.*, the length of the overflow connecting the solution at the tip to the bulk solution in the reservoir) and inversely proportional to the solution flow rate (as flow increases, the cross-sectional area of the overflow increases). To keep the resistance relatively low, the pipette tip was raised only 2 mm above the edge of the reservoir (approximately 3 mm above the reservoir solution when the discharge is operating). The same conductivity meter attached to a Cole-Palmer 1481-62 dip cell was used to measure solution conductivities.

The discharge was imaged 2.3 : 1 with a quartz lens onto the entrance slit of a 0.5-m Czerny–Turner spectrometer (Chromex 500IS/SM (Albuquerque, NM)). The spectrometer could be switched between operation as a monochromator with a PMT detector (Hamamatsu (Hamamatsu, Japan) R928 biased at −850 V) and operation as a spectrograph with a CCD detector (Roper Scientific, Trenton, NJ, Model CH350A). Signals from the PMT were amplified by a Keithley (Cleveland, OH) 427 current amplifier. The output of this amplifier was recorded with a custom National Instruments (Austin, TX) LabVIEW program that also controlled the monochromator. Use of the CCD allowed wavelength resolution in the horizontal direction and spatial resolution in the vertical direction. This vertical position was calibrated by imaging the visible glow of the anode. Images were acquired with WinView/32 (Roper Scientific) and processed with Digital Optics (Auckland, New Zealand) V++ 4.0.

As approximations for the gas-kinetic and electron temperatures, OH rotational and Fe excitation temperatures, respectively, were determined. The OH rotational temperatures were calculated based on the rotational fine structure of the ($A^2\Sigma^+ \rightarrow X^2\Pi_i$) OH band at 306.4 nm by means of a Boltzmann plot.[34] Fe excitation temperatures were calculated similarly from atomic emission lines between 371 and 386 nm.[35]

Results and discussion

Spectral and electrical characterization

To verify that the simplified cell design does not adversely affect its performance, its electrical and spectroscopic characteristics were compared with those published for other designs.

The current–voltage behaviour at discharge gaps from 1–4 mm is shown in Fig. 2. In a normal glow discharge, the voltage stays nearly constant, and the discharge covers an increasing amount of the cathode as current is raised. In contrast, an abnormal glow discharge, the type ordinarily used in atomic spectroscopy, requires a greater voltage in order to produce a higher current because of a restricted cathode area. In the present design, the cathode is completely covered over the entire range of currents used, so the discharge exhibits clearly abnormal behaviour. The degree of abnormality varies among

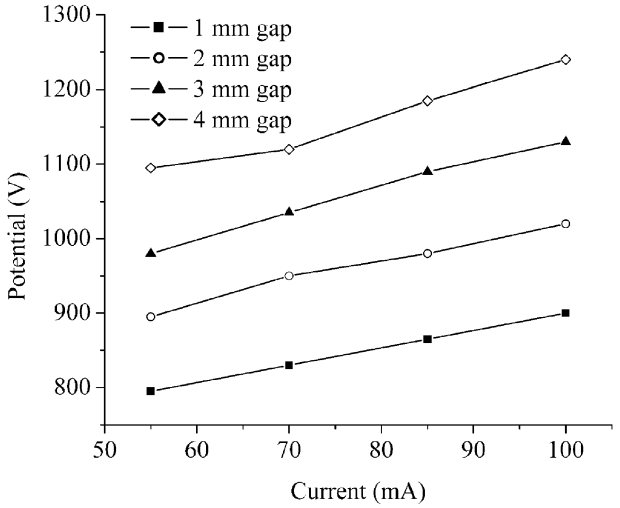

Fig. 2 Effect of discharge current on applied potential for various discharge gaps.

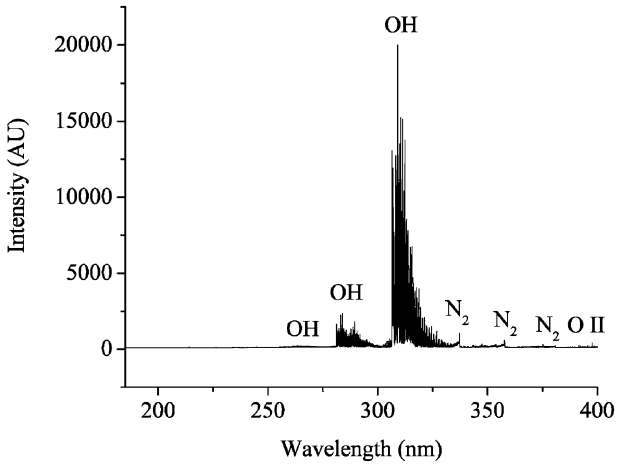

Fig. 3 Background spectrum from 185 to 400 nm. Solution pH = 1, electrolyte = HNO_3, solution flow rate = 3.5 mL min^{-1}, discharge current = 80 mA, discharge gap = 3 mm.

the cells presented in the literature because early devices used a cathode large enough that it was not completely covered by the discharge. Also analogously to a metal–metal glow discharge, the required voltage to maintain a given current increases with the gap between the electrodes. In this system, this trend is linear (Fig. 2).

The continuous-flow limits of detection achieved with the present cell are shown in Table 1 alongside the best values reported in the literature, when available. These values were determined by using a PMT to collect emission from the lower (cathode-side) approximately 2.5 mm of the discharge. Emission from the region above this zone was blocked by affixing electrical tape to the spectrometer entrance slit. As has been previously found,[24] blocking the anode area is useful because of the black body radiation it emits. Additionally, as will be shown, blocking the area immediately below the anode reduces the N_2 background without substantially lowering most analyte emission. Detection limits were calculated based on the variance of the emission from a blank (50 Hz sampling for 10 s) compared with the emission from a solution containing between 100 and 1000 ppb (averaged sampling at 50 Hz over 10 s), depending on the sensitivity of the technique for that element. Similar to other studies,[20] we found that a 2–3 min period was required for stabilisation after initiating the discharge, so we waited at least 8 min between starting the discharge and acquiring data. Also included for comparison are the limits of detection for flow-injection from a recent study.[24] Several literature values have been adjusted to the 3σ definition of detection limits for a fairer comparison. As Table 1 shows, the detection limits found with the present system are comparable to those found with earlier ones.

Likewise, the spectrum of this source (shown in Figs. 3 and 4) resembles spectra found in the literature.[11,12,18,20,22] Unlike for many atomic spectroscopy sources, there is little background emission below 260 nm. Above this wavelength, there are several OH bands, with bandheads at 260.9, 281.1, and 306.4 nm. Next, there is the N_2 second positive system, with bandheads visible from 337.1 to 405.9 nm. Additional bandheads are masked by OH emission at shorter wavelengths. A series of O II lines spreads from 391.2 to 470.1 nm. Beyond this, there are the H_β (486.1 nm) line, the H_α (656.3 nm) line, and three O I lines (777.2, 777.4 and 777.5 nm), as well as Na I

Table 1 Limits of detection for the solution-cathode glow discharge. Solution pH = 1, electrolyte = HNO_3, solution flow rate = 3.5 mL min^{-1}, discharge current = 80 mA, discharge gap = 3 mm, sampling at 50 Hz for 10 s

		LOD (ppb)		
Analyte	Wavelength/ nm	Present work	Best reported	Flow-injection[d]
Cd	228.8	9	30[a]	21
Cu	324.7	31	10[a]	33[e]
Zn	213.9	42	300[b]	24
Pb	368.3	82	10[a]	42[e]
Ni	341.5	110	20[ce]	51
Hg	253.7	349	80[ae]	
K	766.5	13	1[a]	
Mn	279.5	30	30[ce]	
Mg	285.2	19	1200[be]	
Ca	422.7	23	600[b]	
Na	589.0	0.8	1[a]	
Cs	852.1	211		
Ag	338.3	5		
Sr	460.7	49		
Au	242.8	78		
Li	670.8	8		

[a] From ref. 22. [b] From ref. 12, adjusted to 3σ definition. [c] From ref. 21. [d] From ref. 23, adjusted to 3σ definition. [e] Previously used wavelength differs from present work.

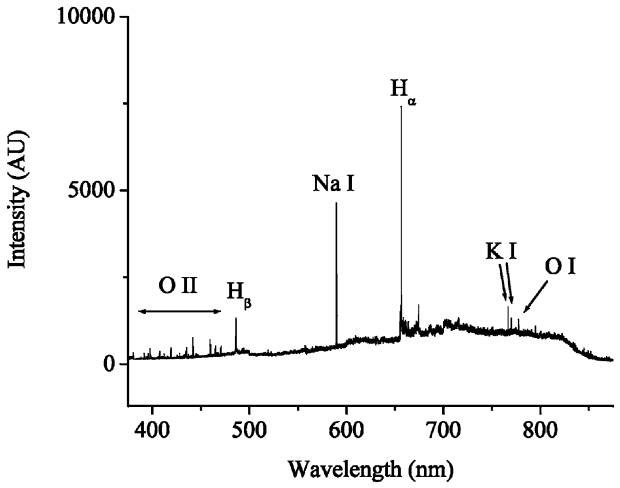

Fig. 4 Background spectrum from 376 to 875 nm. Solution pH = 1, electrolyte = HNO_3, solution flow rate = 3.5 mL min^{-1}, discharge current = 80 mA, discharge gap = 3 mm. A long-pass filter was used from 500 to 655 nm to block second-order radiation at 250 to 327 nm.

(589.0 and 589.6 nm) and K I (766.5 and 769.9 nm) lines from impurities in the blank solution. In Fig. 4, a long-pass filter was used from 500 to 655 nm to block second-order emission from OH.

Vertical distributions of emission and temperatures

In a typical analytical glow discharge there are two regions of strong emission, separated from each other and from the electrodes by regions of weak or no emission. In order, from the anode to the cathode, these regions are the anode dark space, the positive column, the Faraday dark space, the negative glow, and the cathode dark space. The positive column is less intense than the negative glow, but is often spatially much larger. Some parallels can be drawn between these zones and the regions observed in the present source, but there are also significant differences.

The vertical distributions of emission from several background species are shown in Fig. 5. In these profiles, as well as in others, it can be noted that some emission appears to arise from above the anode (positions less than 0 mm) and below the cathode (positions greater than 3 mm). This pattern arises from three factors: the electrodes are cylindrical, so the plasma can, and does, extend around and in front of them; the cathode, being composed of water, is somewhat reflective; and the spatial resolution of the detection system is imperfect.

For the O I and O II traces, the current was 80 mA, the solution flow rate was 3.5 mL min^{-1}, the discharge gap was 3 mm, and the solution was acidified to pH 1.35 with nitric acid. For other species, the conditions were the same except that the current was 85 mA and the flow rate was 3 mL min^{-1}. The N_2 second-positive system bands are most intense near the anode end of the positive column, and their intensity falls off smoothly in both directions. The OH emission intensity shows two regions, the negative glow and the positive column, but no observable Faraday dark space between them. The OH intensity in the positive column reaches nearly three times that of the negative glow. Neutral oxygen also shows two zones of emission, but with a distinct dip between them where the Faraday dark space would appear in a typical glow discharge. Here too, the positive column is more intense than the negative glow, by a factor of about two. Judged by the emission from analyte atoms, which will be shown later, the negative glow peak is near the cathodic edge of that region, and the emission actually extends slightly below the cathode. Singly-charged oxygen shows predominantly one region of emission, also at the cathodic edge of the negative glow. There is weak O II emission in the rest of the negative glow and into the Faraday dark space, but no observable emission in the positive column.

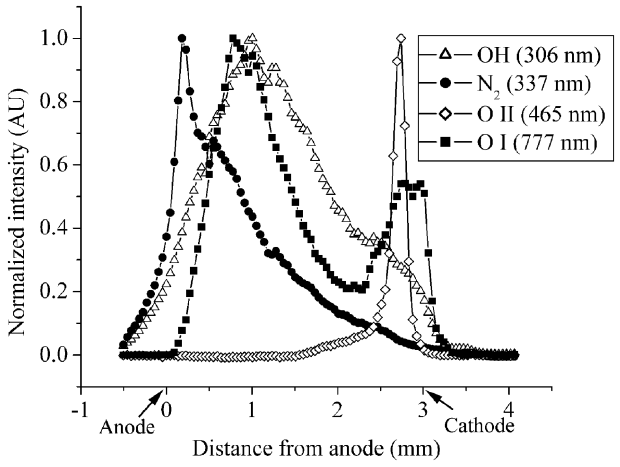

Fig. 5 Vertical distributions of emission from background species. Anode located at 0 mm. Cathode located at 3 mm.

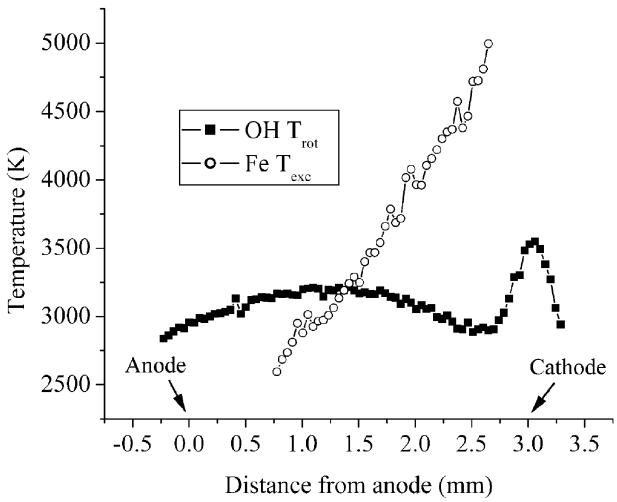

Fig. 6 Typical OH rotational and Fe excitation temperatures. Anode located at 0 mm. Cathode located at 3 mm.

Under the same conditions as were used for measurement of the non-oxygen background species, two temperatures were calculated. The Fe excitation temperature and the OH rotational temperature, the latter of which can be used as an approximation for the gas-kinetic temperature, are shown in Fig. 6. The Fe excitation temperature is shown for only a portion of the gap. Near the anode, N_2 emission interferes with the Fe lines, and near the cathode, below the negative glow, Fe emission is too weak to permit an accurate calculation. It can be seen, however, that the Fe excitation temperature ranges from 2500 K to 5000 K over the observable region, and increases linearly from the anodic edge of the positive column through the negative glow. The OH rotational temperature assumes a somewhat different shape. It peaks near the middle of the positive column, but is fairly constant at roughly 3000 K throughout most of the discharge. Below the negative glow, however, there is an increase in OH temperature to 3500 K that extends to the cathode before falling off. This high temperature near the cathode surface is consistent with that found in experiments and models in low pressure metal–metal glow discharges, which is attributed to this being the region where plasma species putting energy into the discharge gas have their highest energy.[36]

The vertical distributions of emissions from analyte species vary by element and discharge conditions; examples are shown in Figs. 7–9. For these measurements, the discharge current

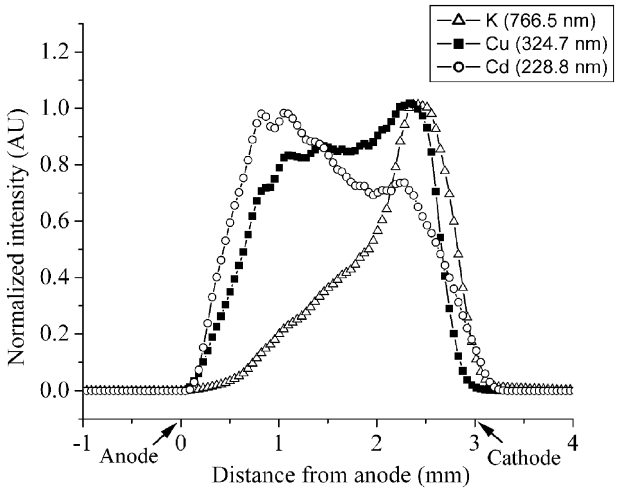

Fig. 7 Vertical distributions of K, Cu, and Cd emissions. Anode located at 0 mm, cathode located at 3 mm.

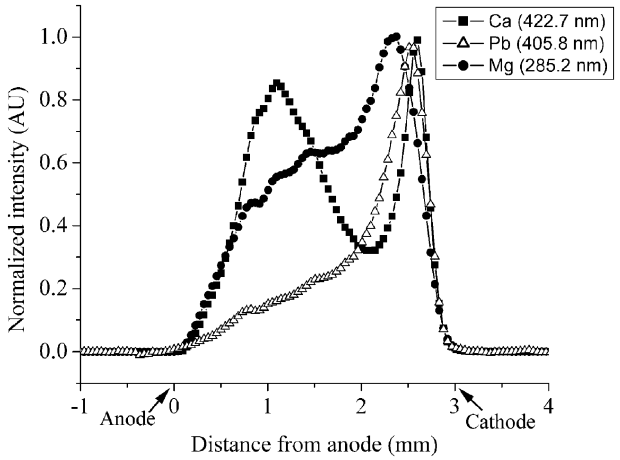

Fig. 8 Vertical distributions of Ca, Pb, and Mg emissions. Anode located at 0 mm, cathode located at 3 mm.

was 90 mA, the discharge gap was 3 mm, the solution flow rate was 3.5 mL min^{-1}, and the solutions were acidified to pH 1.35 with nitric acid. Some elements, such as Ba, Ca, Li, and Sr, exhibit a distinct dip in emission between the negative glow and the positive column in the Faraday dark space. The relative intensities of these two regions vary by element, and the positive column intensity may even be greater than that of the negative glow. Other elements, such as K, Na, and Pb, have intense emission in the negative glow and weaker emission in the positive column, with no distinct dip in emission between these areas. Still others, such as Cu and Cd, have a positive column with intensity comparable to or greater than the intensity in the negative glow. In addition, the positions of the peak negative glow emission and the minimum Faraday dark space emission, when that space is present, can vary by nearly 0.3 mm among elements.

It is important not to assign too much significance to these groupings, both because there are no sharp boundaries among them and because, as will be shown, changing conditions can move some elements from one group to another. The most important conclusions to draw are that the emission distributions vary by element and that the positive column is unexpectedly bright. We hypothesize that this behaviour is related more to transport, desolvation, and atomization than to excitation. It seems likely that a significant portion of the analyte that does not exist as free atoms in the negative glow is atomized in or before the positive column.

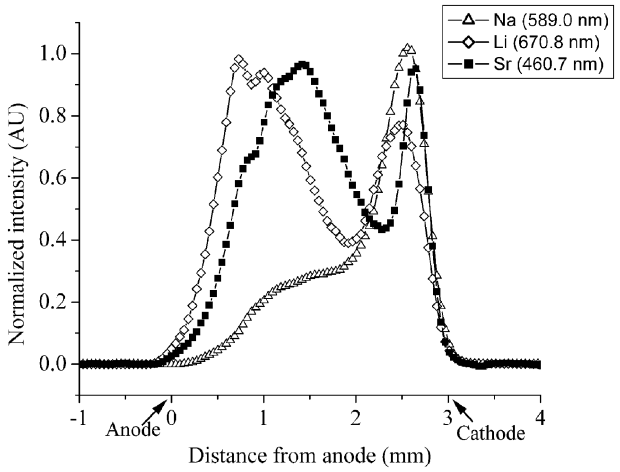

Fig. 9 Vertical distributions of Na, Li, and Sr emission. Anode located at 0 mm, cathode located at 3 mm.

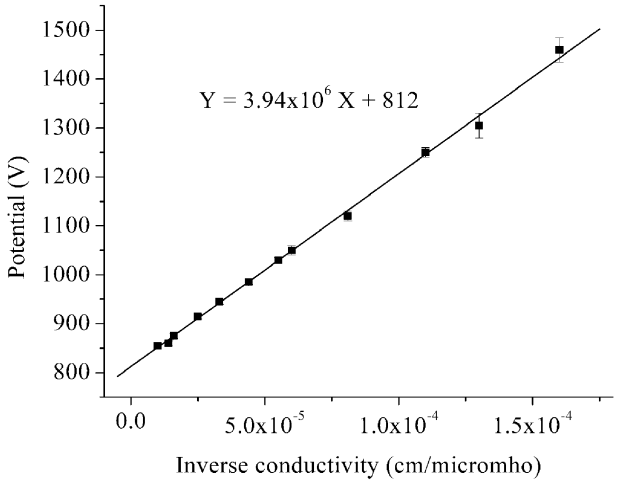

Fig. 10 Effect of solution conductivity on applied potential. Electrolyte = HNO_3, solution flow rate = 3.6 mL min^{-1}, discharge current = 70 mA, discharge gap = 3 mm.

Effect of source conditions on vertical distributions and electrical characteristics

There have been several previous studies on the effects of pH on this type of source.[11–13,18,20,22,26] Overall, the emission was found to grow in intensity with decreasing pH. The apparent discharge voltage was found to rise sharply with pH at low pH values, but to be nearly constant above pH 4.[11] The overall shape was roughly sigmoidal with an inflection point in the vicinity of pH 2.5. This shape has been attributed to a change in the cathode-fall potential with pH, and hypothesized to be the consequence of a two-mechanism system for electron emission, one dominant below pH 2.5 and the other dominant above pH 3.[11,13] It was noted, however, that the voltage drop across the solution (between the discharge and the graphite cathode) was not taken into account in these measurements. Accordingly, before addressing the effect of pH on vertical emission distributions, we should evaluate whether or not it is prudent to neglect this resistance.

A series of solutions adjusted to pH 0.8–1.9 with nitric acid was run through the cell under the same operating conditions (3.6 mL min^{-1}, 3 mm discharge gap, 70 mA), and the potential required to maintain these conditions was measured. These solutions also contained 10 ppm of Cu and Ca, as well as 1 ppm of Na for the studies of vertical emission behaviour that will be described later. The applied voltage was found to be inversely proportional to the solution conductivity and therefore directly proportional to the solution resistance, as shown in Fig. 10. This pattern suggests that the effect of pH on potential is related to a change in the resistance of the solution rather than to a change in the cathode fall potential. To support this hypothesis, it would be desirable to track the trend with conductivity also at higher pH. However, because of its geometry and flow rates, the present system requires a higher potential to maintain a given current than the systems used previously.[11] For this reason, solutions of pH greater than 2 cannot be analyzed. Instead, the conductivities of solutions in the pH range of 1–7.2 were measured, and the voltage that would be required to maintain the discharge was calculated, assuming that the trend found at low pH continued. Because the earlier study[11] used tap water acidified with sulfuric acid, the same was used here to better match that study. Fig. 11 shows the predicted voltage as a function of pH. The potentials are higher due to the different geometry and flow rate, but the overall trend is the same. The graph can be fitted by a sigmoidal function with an inflection point at pH 3.0, near the pH of ~2.5 observed in the earlier study. The difference in

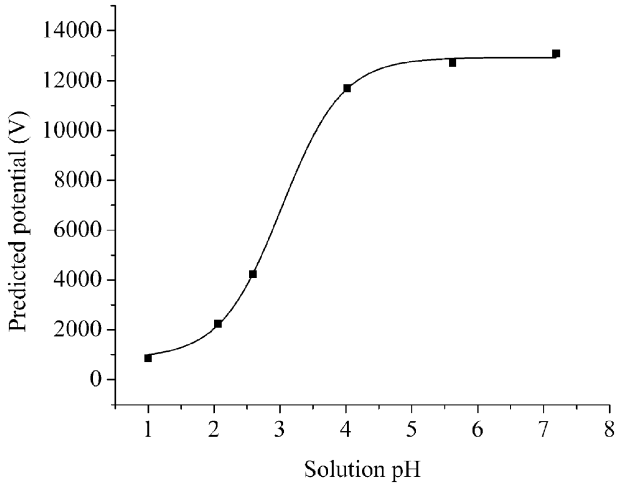

Fig. 11 Predicted required potentials for a range of tap water samples acidified with sulfuric acid.

the initial composition of the tap water and the uncertainty in judging the inflection point visually from the earlier graph are probably responsible for part or all of this difference. The trend of the discharge voltage with pH appears to be attributable to the change in conductivity of the solution rather than to a change in the discharge potential.

No significant differences were found in OH emission intensity, vertical emission distribution, or rotational temperature as pH was varied. Atomic emission, as has been previously reported,[11] goes up as pH is lowered. For Cu and Na, the vertical distribution of emission does not change with pH, but the intensities rise by factors of 5.4 and 6.4, respectively, as the pH drops from 1.9 to 0.8. For Ca emission, the vertical distribution does change, as is shown in Fig. 12. Only four conditions are shown for clarity. Over the pH range from 1.9 to 0.9, the overall emission rises by a factor of 8.0, the negative glow by 20.5, the Faraday dark space by 5.3, and the positive column by 4.2. The result is a transition, moving from pH 1.9 to 0.9, from a pattern of roughly equal positive column and negative glow emission intensities, to one with a distinct dip in between, to one in which the negative glow is nearly five times as intense as the positive column, with no dip in between. At present, the reason for this trend is not clear, but it seems likely that the chemistry of the solution, its conductivity, and/or changes in the negative glow, combine to generate more free atoms in the negative glow at lower solution pH.

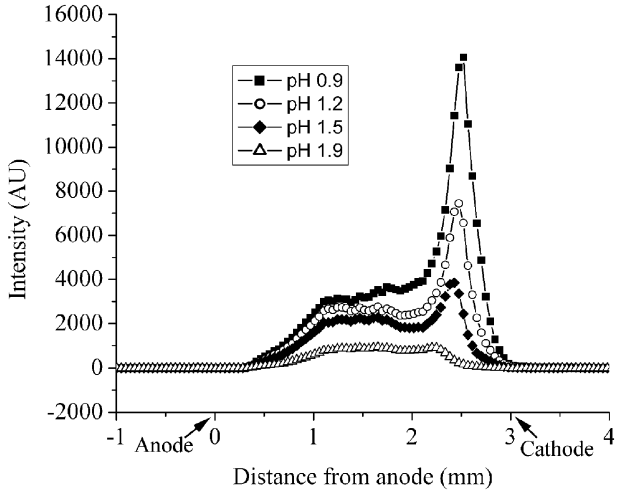

Fig. 12 Vertical distributions of Ca (422.7 nm) emission at different pH values. Anode located at 0 mm, cathode located at 3 mm.

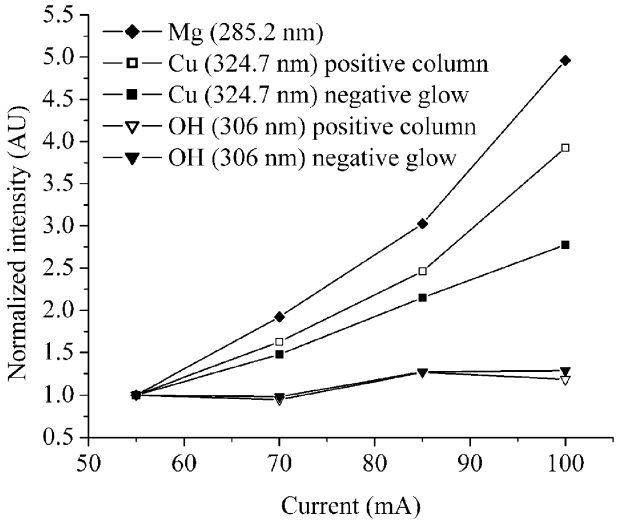

Fig. 13 Typical effects of discharge current on emission. Electrolyte = HNO_3, solution flow rate = 4.0 mL min^{-1}, discharge gap = 3 mm.

Further experiments were performed with solutions acidified to pH 1.35 with nitric acid and containing 10 ppm each of Fe, Mg, and Cu. For these experiments, the current was varied from 55 to 100 mA in 15 mA steps, the discharge gap from 1 to 4 mm in 1 mm increments, and the solution flow rate from 2 to 5 mL min^{-1} in 1 mL min^{-1} steps. Because sample consumption is more rapid at higher discharge currents, experiments with flow rates of 2 mL min^{-1} were performed only at currents of 55 and 70 mA. Owing to spectral interference from N_2 bands, the Fe vertical emission distribution and temperature distributions were not assessed, but the emission distributions of OH, Cu, and Mg were observed, as well as the distribution of the OH rotational temperature. The studied factors were found to be interdependent. For example, a trend found as current is varied (with all other factors held constant) appears slightly different when one or more of those other factors is changed. For this reason, trends are discussed in general terms and largely in a qualitative way, rather than attempting to give an exhaustive quantitative description of each of the many possible conditions observed. To highlight the trends, plots showing typical behaviour due to a variable are shown.

It has been observed previously that atomic emission becomes stronger with increasing current.[11] Fig. 13 shows that similar trends were found in the present work. Although emission from all regions rises with current, the positive column emission goes up more sharply than the negative glow emission, causing the ratio of the negative glow emission to the positive column emission to be smaller at higher currents. At 100 mA, the Cu positive column emission is comparable to or greater than its negative glow emission, and there is a distinct dip between the regions at this current at most flow rates and discharge gaps. The rates of these changes with current vary depending on the other conditions, but the positive column emission typically builds up by a factor of 3–4 as the current increases from 55 to 100 mA and the negative glow emission typically increases by a factor of 2–3 over this range. The positive column emission of Mg is not distinct at low current levels, so that region's rate of increase could not be ascertained, but the Mg negative glow typically rises by a factor of 3–4 over the same current range. The OH emission typically rises by a factor of less than 2 over this range whereas the OH rotational temperature does not change significantly.

The effects of the gap size are similar to those in a more traditional metal–metal glow discharge. Fig. 14 shows typical trends. The analyte negative glow emission is essentially constant at gaps of 2 mm or greater, although it is sometimes more intense at 2–3 mm than at either extreme. The breadth of this

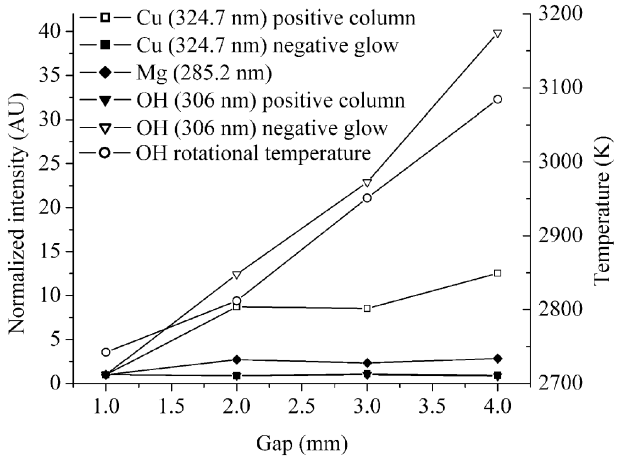

Fig. 14 Typical effects of gap on emission and temperature. OH positive column and Cu positive column are coincident. Electrolyte = HNO_3, solution flow rate = 4.0 mL min^{-1}, current = 85 mA.

region does not change perceptibly with gap sizes from 2–4 mm. The Cu positive column appears as a distinct zone at a gap of 2 mm. For most elements, the intensity in this region is sometimes greatest at a gap of 3 mm, but is typically nearly constant for gaps of 2–4 mm. Only the negative glow region is visible for OH at a gap of 1 mm. At larger gaps, the positive column appears and grows in height with gap size. This region's intensity generally rises with gap, but levels off or declines slightly at 4 mm under some conditions. The OH rotational temperature climbs with gap. As was noted previously, there are two peaks in OH rotational temperature, one below the negative glow and one near the middle of the discharge. The peak near the middle of the discharge typically elevates in temperature from around 2700 K at a gap of 1 mm to 3200 K at a gap of 4 mm. As the gap grows, the potential required to maintain a given current becomes larger. This temperature increase is due to the higher power dissipated across a larger gap. The peak below the negative glow, however, is roughly constant at 3600 K.

The solution flow rate has a significant impact on the emission, but the OH rotational temperature does not vary with flow rate. Fig. 15 shows typical behaviour. Overall, the OH emission strengthens with flow. The atomic emission generally increases with flow, then levels off or declines above 3–4 mL min^{-1}. The negative glow shifts slightly closer to the anode as flow rises, as a consequence of the cathode surface moving upwards. At a current of 70 mA and a gap of 4 mm, this shift is on the order of 0.08 mm between a flow rate of 2 mL min^{-1} and one of 5 mL min^{-1}. As the surface moves upwards, the exposed surface area becomes larger as well. It may be that this greater surface area raises the amounts of both water and analyte that enter the discharge, explaining the increase in atomic emission from 2–4 mL min^{-1} and the greater OH emission with higher flow. The levelling off or reduction in atomic emission at higher flows may also be a consequence of additional water vaporization. This water or its products might solvate or otherwise bind atoms, or they may reduce the energy or number of electrons available for exciting the atoms.

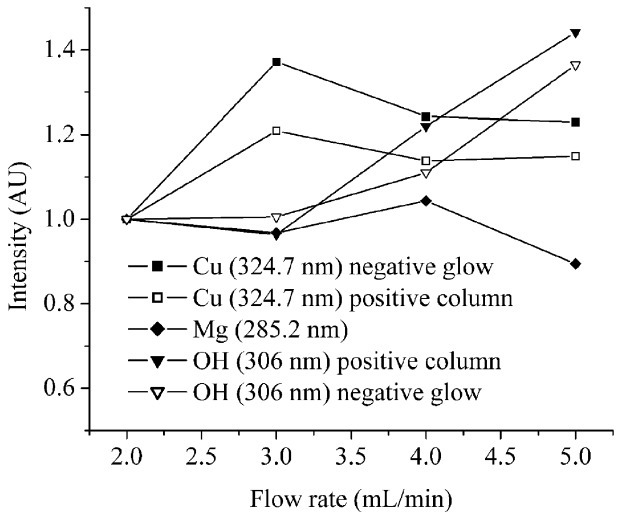

Fig. 15 Typical effects of flow rate on emission. Electrolyte = HNO_3, discharge gap = 3 mm, current = 70 mA.

Conclusions

A glow discharge using a solution as the cathode shows promise as a sensitive and inexpensive technique for the elemental analysis of liquids. A better understanding of the effects of various parameters on the discharge can help with optimizing the discharge on a phenomenological basis and, if these effects can be understood on a more fundamental level, a mechanistic basis. The analyte and background profiles offer promise that better signal-to-noise ratios could be achieved for certain elements if emission were collected only from certain areas; however, the variations among the emission distributions of different elements limit the feasibility of this approach if ELCAD is to be used as a multi-elemental technique. Collecting emission from all but the zone 0.5 mm closest to the anode might (as was done here) offer a good compromise and is readily accomplished due to the small size of the discharge. Although the mechanisms within such a discharge are still unclear, the emission has now been shown to vary both in intensity and in vertical distribution with pH, current, solution flow rate, discharge gap, and element. This emission has also been shown to have distinct regions. The relative intensities of these regions and their responses to the various parameters studied suggest that a significant fraction of the emission for many elements is not from atoms ejected by sputtering from the solution, as has been suggested,[15] but from metals desolvated and atomized some distance above the solution.

Acknowledgements

This research was supported by the US Department of Energy through Grant DE-FG02-98ER14890.

References

1 R. K. Marcus and J. A. C. Broekaert, *Glow Discharge Plasmas in Analytical Spectroscopy*, Plenum, 2003.
2 T. K. Starn, R. Pereiro and G. M. Hieftje, *Appl. Spectrosc.*, 1993, **47**, 1555.
3 C. L. Lewis, M. A. Moser, D. E. Dale, Jr., W. Hang, C. Hassell, F. L. King and V. Majidi, *Anal. Chem.*, 2003, **75**, 1983.
4 W. O. Walden, W. Hang, B. W. Smith, J. D. Winefordner and W. W. Harrison, *Fresnius' J. Anal. Chem.*, 1996, **355**, 442.
5 C. M. Strange and R. K. Marcus, *Spectrochim. Acta, Part B*, 1991, **46**, 517.
6 S. G. Schroeder and G. Horlick, *Spectrochim. Acta, Part B*, 1994, **49**, 1759.
7 J. Gubkin, *Ann. Phys. Chem.*, 1887, **32**, 114.
8 D. E. Couch and A. Brenner, *J. Electrochem. Soc.*, 1959, **106**, 628.
9 T. Suzuki, Y. Matsushima, Y. Mori, T. Yamazaki and T. Noma, *J. Mater. Sci.*, 2002, **37**, 595.
10 A. M. Kutepov, A. G. Zakharov, A. I. Maksimov and V. A. Titov, *High Energy Chem.*, 2003, **37**, 317.
11 T. Cserfalvi, P. Mezei and P. Apai, *J. Phys. D*, 1993, **26**, 2184.
12 T. Cserfalvi and P. Mezei, *J. Anal. At. Spectrom.*, 1994, **9**, 345.
13 T. Cserfalvi and P. Mezei, *Fresenius' J. Anal. Chem.*, 1996, **355**, 813.
14 T. Cserfalvi, *Magy. Kem. Lapja*, 1997, **52**, 502.
15 P. Mezei, T. Cserfalvi and M. Janossy, *J. Anal. At. Spectrom.*, 1997, **12**, 1203.

16 P. Mezei, T. Cserfalvi and M. Janossy, *J. Phys. D*, 1998, **31**, L41.
17 P. Mezei, T. Cserfalvi, M. Janossy, K. Szocs and H. J. Kim, *J. Phys. D*, 1998, **31**, 2818.
18 Y. S. Park, S. H. Ku, S. H. Hong, H. J. Kim and E. H. Piepmeier, *Spectrochim. Acta, Part B*, 1998, **53B**, 1167.
19 S.-H. Chang, H.-J. Kim, S.-T. Kim and Y.-M. Kim, *Anal. Sci. Technol.*, 1999, **12**, 299.
20 H. J. Kim, J. H. Lee, M. Y. Kim, T. Cserfalvi and P. Mezei, *Spectrochim. Acta, Part B*, 2000, **55B**, 823.
21 P. Mezei, T. Cserfalvi, H. J. Kim and M. A. Mottaleb, *Analyst*, 2001, **126**, 712.
22 M. A. Mottaleb, Y. A. Woo and H. J. Kim, *Microchem. J.*, 2001, **69**, 219.
23 M. A. Mottaleb, J. S. Yang and H.-J. Kim, *Appl. Spectrosc. Rev.*, 2002, **37**, 247.
24 T. Cserfalvi and P. Mezei, *J. Anal. At. Spectrom.*, 2003, **18**, 596.
25 A. I. Maksimov, V. A. Titov and A. V. Khlyustova, *High Energy Chem.*, 2004, **38**, 196.
26 V. V. Yagov and M. L. Gentsina, *J. Anal. Chem.*, 2004, **59**, 64.
27 W. C. Davis and R. K. Marcus, *J. Anal. At. Spectrom.*, 2001, **16**, 931.
28 R. K. Marcus and W. C. Davis, *Anal. Chem.*, 2001, **73**, 2903.
29 W. C. Davis and R. K. Marcus, *Spectrochim. Acta, Part B*, 2002, **57**, 1473.
30 K. K. Tazmeev and B. K. Tazmeev, *J. Eng. Phys. Thermophys.*, 2003, **76**, 868.
31 C. J. Herring and E. H. Piepmeier, *Anal. Chem.*, 1995, **67**, 878.
32 G. Jenkins and A. Manz, *J. Micromech. Microeng.*, 2002, **12**, N19–N22.
33 Y. Matsushima, A. Tezuka, K. Sumida, K. Maeda, T. Noma, T. Yamazak and T. Suzuki, *J. Mater. Sci. Lett.*, 2003, **22**, 1259.
34 U. Engel, C. Prokisch, E. Voges, G. M. Hieftje and J. A. C. Broekaert, *J. Anal. At. Spectrom.*, 1998, **13**, 955.
35 Y.-i. Sung and H. B. Lim, *J. Anal. At. Spectrom.*, 2003, **18**, 897.
36 A. Bogaerts, R. Gijbels, G. Gamez and G. M. Hieftje, *Spectrochim. Acta, Part B*, 2004, **59**, 449.